COBEM 2021 26th International Congress of Mechanical Engineering
November 22-26, 2021, Virtual Congress, Brazil

COB-2021-1953
DETERMINATION OF INSTALLATION SITES OF HYDROKINETIC TURBINES DOWNSTREAM OF THE SEFAC HYDROELECTRIC FACILITY

Kaajal Gopie
Isadora Montenegro Bugarin
Rafael Castilho Faria Mendes
Taygoara Felamingo de Oliveira
University of Brasília, Faculty of Technology, Laboratory of Energy and Environment.
kaajal.gopie@aluno.unb.br; isadorabugarin@gmail.com; rafael.cfmendes@gmail.com; taygoara@unb.br

Abstract. *The hydrokinetic potential of electricity generation from a river stretch is studied using the numerical methods for turbulent flows. We simulated a turbine farm along a portion of the São Marcos river, downwind the dam of the SEFAC hydroelectric facility. The geometric data of the natural channel was generated by field experiments using Acoustic Doppler Current Profiler (ACDP) methods. The flow boundary conditions were defined by considering the actual flow rate of the facility. The numerical methodology was verified using experimental data for sinusoidal open channel flow available in the literature. Different turbulent models are tested. The free surface is simulated considering a slipping boundary. We use the simulations to look for useful sites for hydrokinetic unit installations, considering the local flow velocity, secondary currents occurrence, and turbulent kinetic energy levels.*

Keywords: *hydrokinetic potential, numerical simulation, turbine sites*

1. INTRODUCTION

In a world with depleting fossil fuels reserves and an increased greenhouse effect, the existence of renewable energy resources takes on a significant role in providing energy. These resources are not only sustainable, and as their name itself suggests, renewable, but are also environment friendly. Of all known renewable energy sources, hydropower would be the most efficient and largest resource (S.A., 2015; Barta *et al.*, 2011; Office, 2021; Laws and Epps, 2016). One method to generate energy from water is via hydrokinetic technology (Yuce and Muratoglu, 2015). This type of energy conversion device eliminates the need for the construction of a dam or water reservoirs for hydroelectric facilities, as they need no or little elevation to generate energy (Khan *et al.*, 2009). These systems simply convert the kinetic energy present in flowing water into electric energy (Güney and Kaygusuz, 2010). As the water flowing downstream of hydroelectric facilities often enough still has a kinetic potential, the available energy can be exploited by installing hydrokinetic turbines downstream of the facility.

In order to implement the hydrokinetic technology, the available hydrokinetic energy potential in the waters of where the system is to be used must be studied thoroughly (Liu and Packey, 2014). As in this paper this technology is to be implemented ultimately in a natural channel, the flow behavior of such a channel will be studied. The biggest challenge in estimating the hydrokinetic potential in a natural channel is the difficulty in modeling the flow field (da Silva Holanda *et al.*, 2017). The flow structure of an open-channel flow is complex and varying, as a three-dimensional (3D) interaction between takes place between the fluid, channel walls and bed. This interaction involves especially parameters as gravity, turbulence and roughness. The combination of these factors make the study of open channel flow challenging. However, by using computational fluid dynamics (CFD), this problem can be resolved with a more complete and detailed modeling of the channel and fluid flow analyzation (Santos *et al.*, 2019; Knight *et al.*, 2005).

Over the years, a rising amount of researches have been dedicated to the study of open-channel flow in artificial channels by numerical simulation (Sahoo *et al.*, 2020; Blanckaert and Graf, 2001; Tang *et al.*, 2015). The artificial channels are specifically constructed to imitate natural flow behavior. The majority of the researches utilize Reynolds Averaged Navier Stokes (RANS) turbulence models to generate results. In the article written by Kamel *et al.* (2014), an attempt is made to develop a numerical method to predict the flow in river bends (curves). The bends have various curvatures and width-depth ratios. Their method uses the 3D non-linear k-ϵ model for a meandering compound channel with a rectangular cross-section. As this turbulence model managed to successfully predict the flow structures and velocity distributions along the channel, makes it possible to be applied for natural channels. This model also managed to demonstrate the presence of an important feature in natural channels: secondary currents. These currents have a noticeable effect on the

flow structures and are caused by turbulence anisotropy. Two other works that also managed to demonstrate the presence of secondary currents are that of Jing *et al.* (2009) and Jing *et al.* (2011). Both studies used the Reynolds Stress Model (RSM) to simulate the flows in compound channel meandering flows with different cross sections. The study conducted by Jing *et al.* (2009) simulates the channel with a semi-natural cross section, while the research by Jing *et al.* (2011) apply the RSM to a channel with a trapezoidal cross section. Both studies show a thorough analysis of the secondary flow by varying water depths. Furthermore, the results are in concordance with experimental data, making the RSM one more turbulence model suitable for predicting natural channel flow.

In this case of modeling a natural channel for CFD simulations, information about the velocities, depths, and relief of the river, in other words, the bathymetry of the channel is required. Modeling the channel will allow for determining high velocity areas along with suitable locations for the turbines, after which the hydrokinetic potential can be estimated (Holanda *et al.*, 2017). The entire process of modeling the channel up till determining the energy potential consists of an extensive numerical investigation, of which the results are presented in this work.

2. NUMERICAL METHODOLOGY

The first step in this numerical investigation process is the validation of the proposed methodology. Once the method is validated, the research progresses to numerical simulations with the computational mesh generated using bathymetric data.

2.1 Methodology validation

For the validation, an artificial channel with natural channel characteristics, a benchmark channel, is chosen and turned into a computational mesh. The generated results are compared to experimental results. A suitable geometry was encountered in model FCF-23B (Fig.1). This experimental model is installed in the Science and Engineering Council Flood Channel Facility (SERC FCF). This facility has been especially constructed for research in the hydraulic behavior of rivers and flood alleviation channels for when the water flows out of the bank (Knight and Sellin, 2007). The benchmark channel has a trapezoidal cross section with a slope of 45°, also seen in Fig. 1.

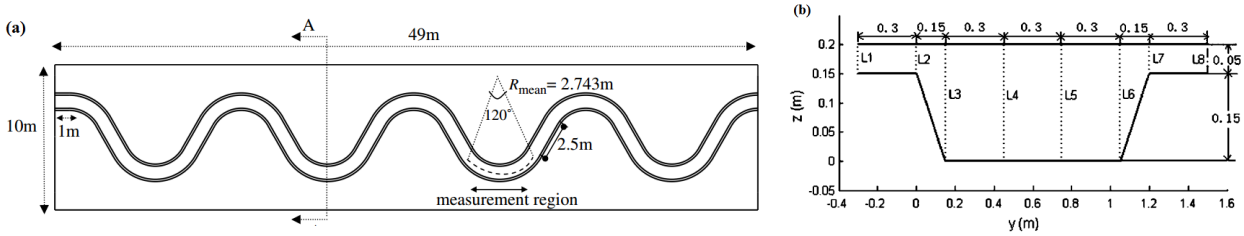

Figure 1. Benchmark channel geometry with a cross over of 60°(a) by Farshi *et al.* (2018) with the cross section (b) by Jing *et al.* (2011).

The mesh has been generated in ANSYS meshing using tetrahedral elements with a linear global element order of 0.05 m. For the walls (including the bottom of the channel), the inflation layer option was utilized, with 15 layers and a first layer size of 3.8×10^{-4} m. The generated mesh has 3053323 nodes and 6973984 elements with an average y^+ of 7.28.

For the simulation, case 3 of Jing *et al.* (2011) has been considered. The details of this case can be found in Tab.1.

Table 1. Case 3 inlet values by Jing *et al.* (2011).

DR	**Q (m^3/s)**	**H (m)**	**U_{in} (m/s)**	**k_{in} (m^2/s^2)**	**ϵ_{in} (m^2/s^3)**
0.25	0.2480	0.2	0.378	2.14×10^{-3}	8.14×10^{-4}

The kinetic energy turbulence k_{in} and its dissipation rate ϵ_{in}, evaluated by (Choi and Kang, 2008; Guo *et al.*, 2009; Jing *et al.*, 2009), are calculated respectively by Eq. (1) and Eq. (2)

$$k_{in} = \frac{3}{2}(IU_{in})^3, \tag{1}$$

$$\epsilon_{in} = c^{3/4}\mu\frac{k_{in}^{3/2}}{0.1R}, \tag{2}$$

in which I is the turbulence intensity, assumed to be 10% and R is the hydraulic radius.

At the inlet, the average velocity $\mathrm{U_{in}}$ is determined with $\mathrm{U_{in}} = \mathrm{Q}/\mathrm{A}$, in which Q is the flow rate and A the cross sectional area of the inlet.

The relative water depth DR is defined as the ratio between water depth over the flood plain (h) and the maximum water depth in the main channel (H).

At the inlet, a velocity of $\mathrm{U_{in}}$ as given in Tab.1 has been set. At the outlet, the condition of a static pressure equal to zero has been defined. The walls have a non-slip condition, while the free surface is modeled as a slip wall. The simulations are carried out using ANSYS CFX software.

The mesh is further configured with a convergence study retaining the same boundary conditions and using the k-ϵ model. The mesh is successively refined with an increasing number of nodes.

In order to verify which turbulence model is able to simulate consistent results closest to the experimental data, simulations with unchanged boundary conditions with three models (a turbulence model performance study) are carried out: the RSM, the k-ϵ and the k-ϵ EARSM model.

Ultimately, the methodology validation is realized by comparing results of the most accurate turbulence model in the turbulence model performance study with experimental data by de Lima da Silveira e Lorena (1992).

2.2 Bathymetric data acquisition methodology

The river geometry (bathymetry) is based on depth measurements carried out with a Sontek M9 device, an Acoustic Doppler Current Profiler (ADCP). This tool generates an ultrasonic acoustic wave into the water and detects the backscatter's time from the river bottom and small particles. Following the doppler effect principles, makes it possible to compute the depth and the velocity components over the measured water column. The ADCP was assembled in a boat, as shown in Fig. 2, and was driven along the river. Under this assemble, the data was obtained following the trajectories presented in Fig. 3.

Figure 2. Boat (a) with the ADCP assembly (b).

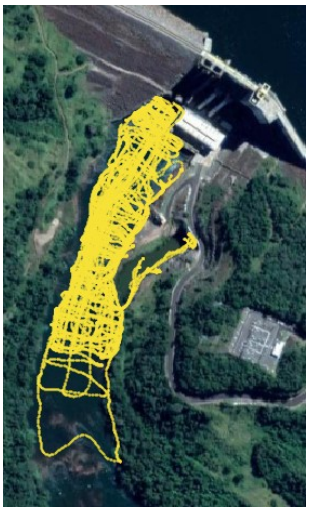

Figure 3. Boat trajectories on the channel taken for the measured depth.

2.3 Numerical simulation using bathymetric data

After the methodology validation and the bathymetric data acquisition, the last phase of the investigation is realized. Using the bathymetry, the computational mesh shown in Fig. 4 has been designed. This channel has a length of approximately 345.27 m with a varying depth and channel width.

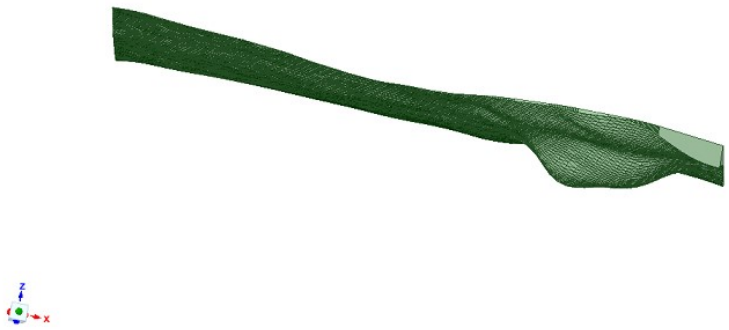

Figure 4. Computational discretized mesh of the SEFAC channel.

The geometry has been designed in ANSYS Spaceclaim with an inlet, outlet, a free surface plane and channel walls. The free surface plane is placed at a zero water level.

The mesh has been generated using tetrahedral elements with a linear global element order size of 0.5 m. The resulting mesh consists of 788902 nodes and 3947129 elements.

At the inlet, a flow rate condition of 91 m^3/s has been placed. For the remaining three conditions the same boundary conditions as described for the validation method are considered. The same three turbulence models used in the turbulence model performance study, will be used for the simulations, in order to discover whether these models are able to predict the flow structures in a natural channel as well as for the artificial channel. These simulations are also carried out using ANSYS CFX software.

3. RESULTS

This section presents the results obtained from employing the methodology described in the previous section.

3.1 Mesh convergence study of the benchmark channel

For the mesh convergence study, the mean velocity $\mathrm{U}_{\mathrm{mean}}$ has been plotted against an increasing number of nodes. Fig. 5 presents the results of this study. The graph shows the results of four mesh resolutions, with the mesh refined to almost 2.5 million nodes.

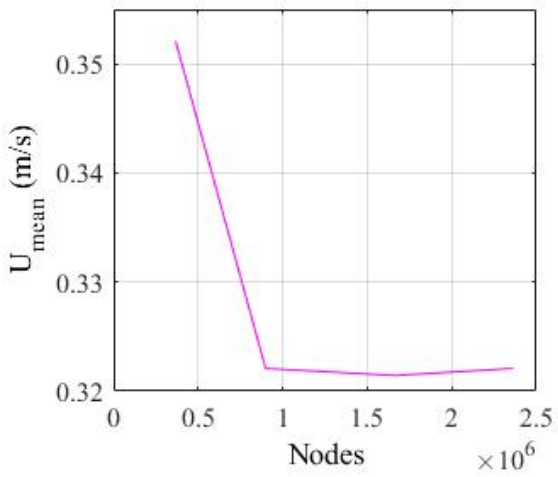

Figure 5. Mesh convergence of the benchmark channel for $\mathrm{U}_{\mathrm{mean}}$.

The mean velocity starts out high, decreasing to lower steady values. The graph shows a steady behavior for the last three mesh resolutions, signifying convergence. This convergence proves that the solution of the simulation is independent

of the mesh resolution.

3.2 Turbulence model performance study for the benchmark channel

The turbulence model performance study has been conducted for two regions of the cross section presented in Fig. 1: L3 and L5, of which the results are presented in Figures 6 and 7. The axis limits have been adjusted specifically to emphasize the difference in the results of the models. The experimental data has also been plotted only to show whether or not the numerical data shows a similar velocity profile pattern and if so, which model shows the most similar and consistent graph pattern. From there on, the comparison between the best performing model and the experimental data is presented in section 3.3.

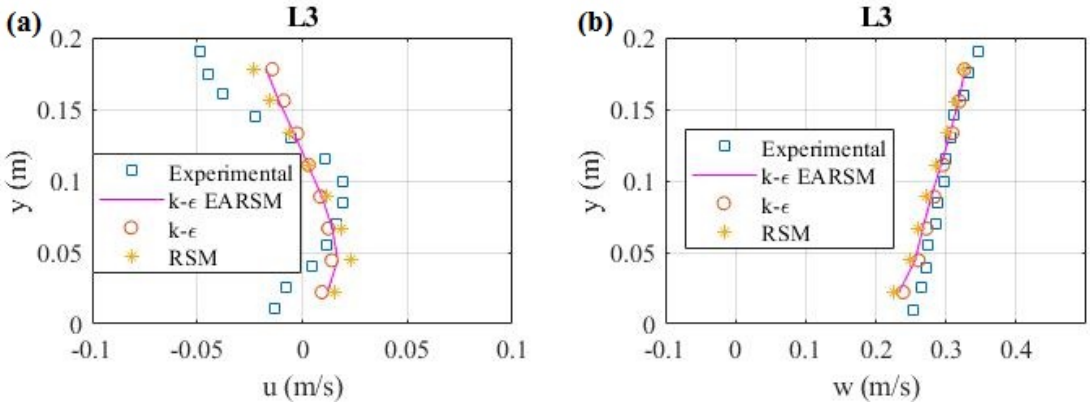

Figure 6. Turbulence model performance comparison plotted with experimental results for transverse velocity u (a) and longitudinal velocity w (b) for L3.

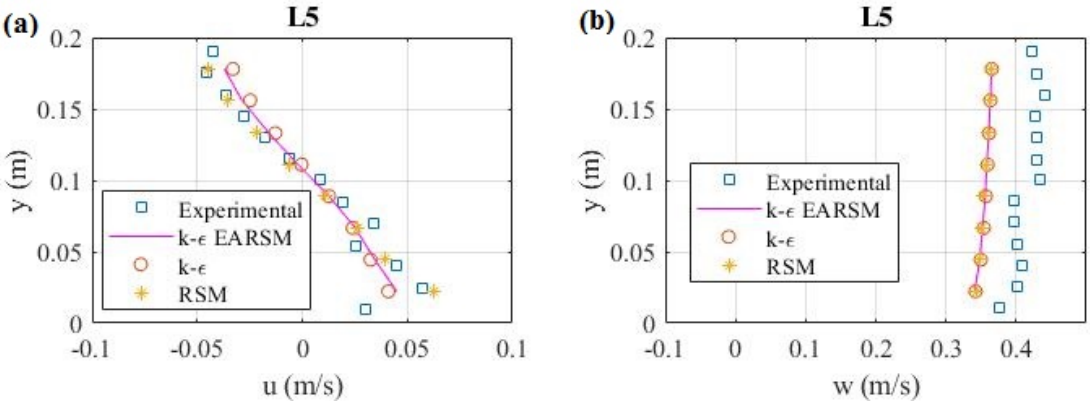

Figure 7. Turbulence model performance comparison plotted with experimental results for transverse velocity u (a) and longitudinal velocity w (b) for L5.

Despite all three models demonstrating a similar velocity profile for all four graphs, the variations in the data can be visualized in three out of four graphs. The only graph where the plotted data of all three models show the highest concordance, is where the numerical velocity profiles differ the most from the experimental profile, which is seen in Fig. 7. Studying the three remaining graphs, shows the RSM displaying the most consistent and similar to experimental velocity profiles, making it suitable to use for the methodology validation.

3.3 Methodology validation

Finally, the methodology has been validated comparing the experimental results with results from the simulation with the RSM. Figures 8 and 9 present the validation results for the u and w for three regions of the main channel. All graphs featured in Fig. 8 show a good concordance between simulated and experimental results. However, in the case of Fig. 9, only one graph shows a good concordance between both results. The discordance between experimental and numerical results is the greatest for the longitudinal velocities, but even so, the velocity profile pattern behavior is maintained by the numerical data. This discordance may have been caused by a complex flow interaction between the floodplain and main channel, as both L4 and L5 are in the middle of the channel cross section and they would be influenced the most by floodplain flow and main channel flow interaction. With the majority of the velocity profiles showing a good agreement

between experimental and numerical data, the proposed methodology is deemed capable of reproducing the flow in a meandering compound channel.

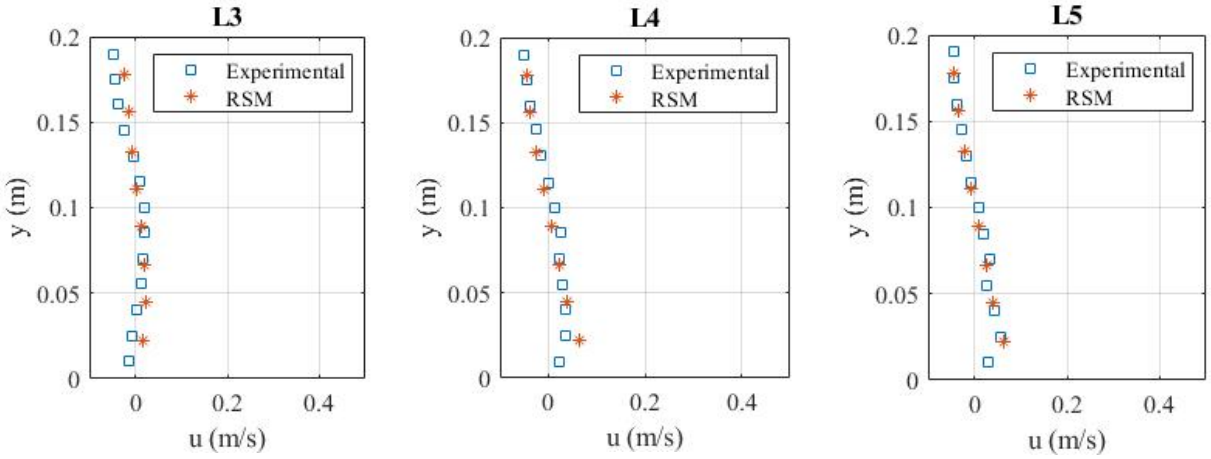

Figure 8. Comparison between experimental and RSM results for transverse velocity u.

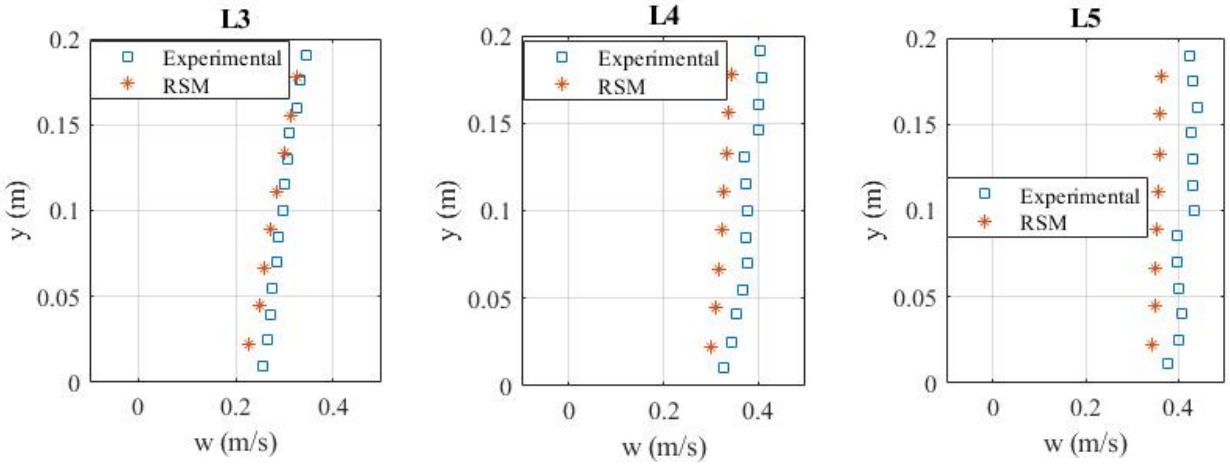

Figure 9. Comparison between experimental and RSM results for longitudinal velocity w.

3.4 SEFAC channel simulation results

3.4.1 Potential turbine sites

In order to locate potential locations for the turbines, areas of high velocities and large depths must be analyzed. Studying both the velocity and depth contours of the channel, presented in Fig. 10, allows for choosing sections of the channels, where both requirements can be satisfied. The aim is to find areas with a velocity starting from 1 $\mathrm{m/s}$ and a depth of 2 m and higher. Ultimately, five sections seemed to fulfill these requirements. In Fig. 10, these five sections, colored with black, made in the channel for further analysis, are presented. The sections in the channel span across the whole channel width. As there are no significant differences in results in terms of contour maps, all contour maps will be given for the same turbulence model (k-ϵ) in order to keep a consistency in the results.

In each section, four velocity profiles have been chosen (at areas with high velocity and great depth), equally spaced from each other and defined as regions P1 to P4 per section. The potential areas are encountered in the middle of the channel. The search for the installation sites starts with 20 potential locations.

A major consequence of great turbulence are recirculating secondary currents. Finding these currents in one of the sections would help narrow down the number of potential sites. As the currents simulated by the models do not differ greatly, only the currents for the k-ϵ model are presented in Fig. 11 for all five sections, focused on the area of the potential installation sites.

As Fig. 11 presents no recirculating secondary flow occurrence, the potential turbine sites shall have to be analyzed and narrowed down further by studying the turbulence intensity only. As all turbulence intensity profiles have the same graph pattern, with the only differences being in depth and intensity value, only the profiles with a turbulence intensity

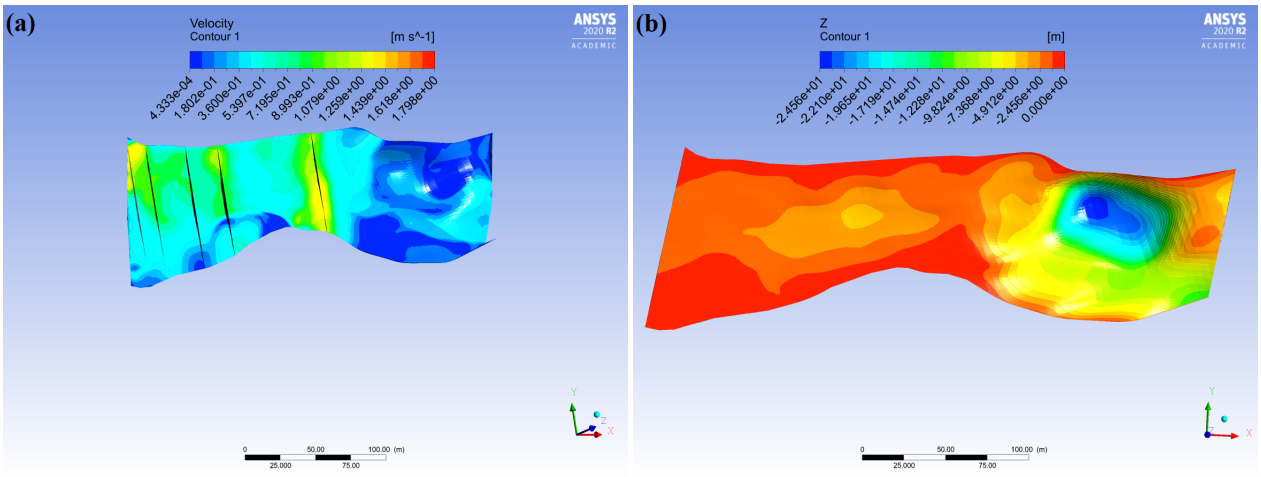

Figure 10. Velocity (a) and depth (b) contours over the SEFAC channel obtained by simulations with the k-ϵ model.

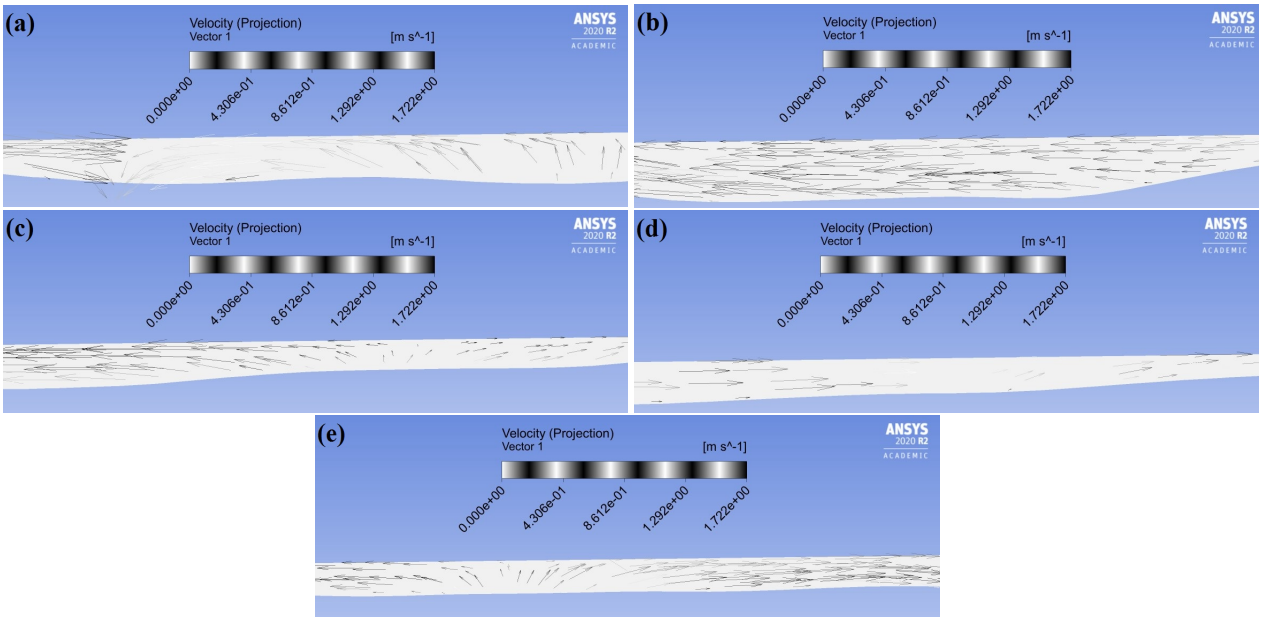

Figure 11. Secondary currents for sections 1 (a), 2 (b), 3 (c), 4 (d) and 5 (e) obtained by simulations with the k-ϵ model.

extremely close to or higher than one are shown in Fig. 12. An intensity of higher than one, would mean a high turbulent kinetic energy level at that site, according to the definition of turbulence intensity.

The turbulence intensity varies from approximately 0.2 to slightly higher than 10 over all profiles. The depths vary from approximately 1.4 m to 3 m. The aim is to encounter only sites with a depth of more than 2 m, but sites of 1.4 m depth could also be suitable sites for the turbine. Logically, the site with an intensity of 10, at section 3 P2, would make an excellent site. The depth and turbulence intensity are more than adequate. As all chosen turbulence intensity profiles have a suitable depth and turbulence intensity profile, all the regions presented in Fig. 12 can be presented as potential hydrokinetic turbine installation sites.

A fact worth mentioning is that when comparing the results of the turbulence models with each other, the RSM deviates the most in results. The calculated turbulent intensities for RSM are extremely small, the smallest I not even attaining a value of 0.05.

3.4.2 Flow in depression area

In Fig. 11 could clearly be seen that no recirculating flow is to be found in any of the sections. This may have to do with the river bed not being deep enough for recirculating currents. There is however, another area, right after the inlet in the channel, where recirculating flow is certainly to be expected. Unfortunately, this area could not possibly be a potential installation site for the turbines, as the velocity there is the lowest, according to Fig. 10. Despite its unsuitability as an installation site, this depression of 24.5 m in the channel bed does create an interesting situation in the channel flow, featured in Fig. 13.

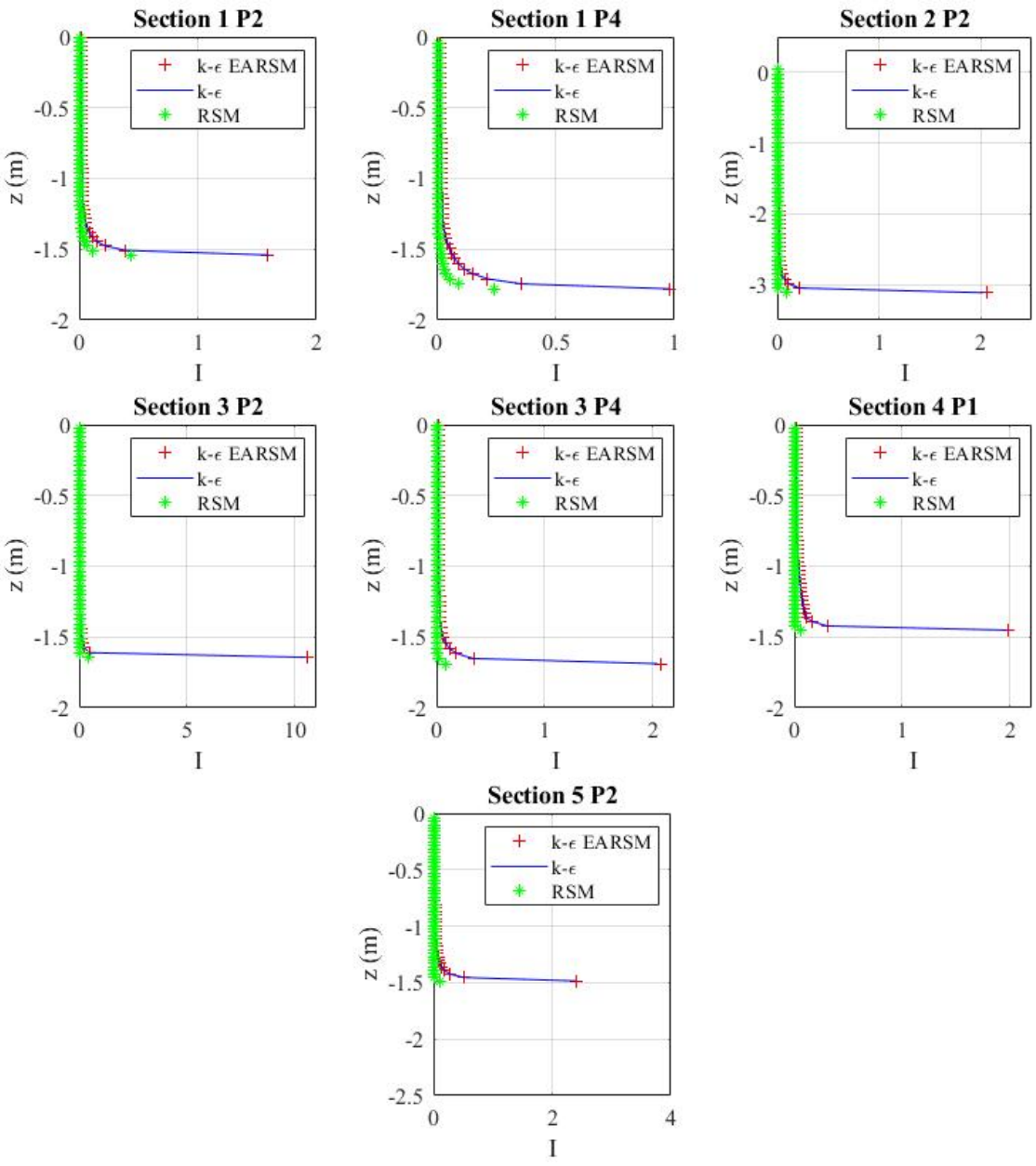

Figure 12. Turbulence intensity profiles of the three turbulence models with highest turbulence intensities.

The transverse velocity is over the whole depression area constant. The flow after the depression area has a lower transverse velocity than is found in the depression itself. This type of depression can be depicted as a type of driven cavity flow. The water flow on the upper surface of the depression creates a shearing force, moving the fluid in the cavity, resulting in a primary vortex and smaller vortices as a result of changes in the wall. In a standard driven cavity flow case, the transverse velocity on the upper surface would be the highest and in the depression the lowest. In the current case, a different result is found, as it is not a standard cavity flow. The depression is not uniformly deep and the fact that it is located right after the inlet may influence the transverse velocity. The main vortex develops in the deepest area of the depression and the smaller vortices in the shallower parts. Despite the differences in transverse velocities between the standard case and the current case, the depression in the SEFAC channel, manages to develop the vortices, which shows a fundamental similarity between both cases.

4. CONCLUSION

In this paper, it has been proven that the proposed methodology of simulating natural channel flow is possible and its results are proven to be accurate. The results from simulating the SEFAC channel show five sections along where possible turbine sites could be located. However, as a result of the missing presence of rotating secondary currents, the potential sites can only be further analyzed for eligibility based on the highest turbulence intensities. Following this analysis, seven

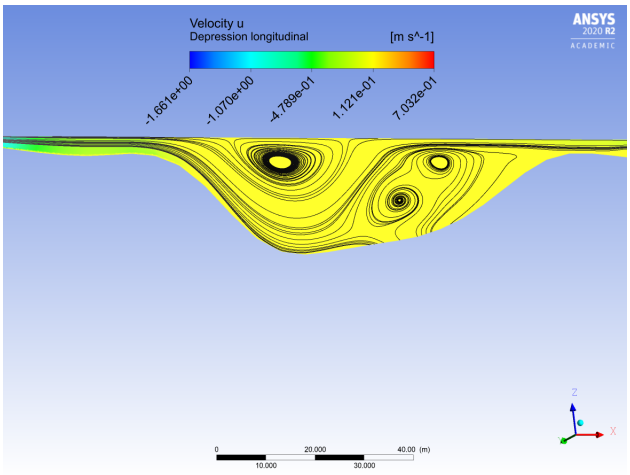

Figure 13. Transverse velocity u contours with streamlines for the cross section in depression area obtained by simulations with the k-ϵ model.

sites are deemed highly suitable as turbine installation sites.

5. ACKNOWLEDGEMENTS

The authors would like to thank Serra do Facão Energia S.A. for providing financial support for the development of the project (ANEEL:P&D06899-2002/2020) - Desenvolvimento de metodologia para determinação de potencial de energia hidrocinética em usinas hidroelétricas.

6. REFERENCES

Barta, B., Van Dijk, M. and Van Vuuren, F., 2011. "Renewable energy: hydropower". *Civil Engineering= Siviele Ingenieurswese*, Vol. 2011, pp. 37–41.

Blanckaert, K. and Graf, W.H., 2001. "Mean flow and turbulence in open-channel bend". *Journal of Hydraulic Engineering*, Vol. 127, pp. 835–847.

Choi, S. and Kang, H., 2008. "Reynolds stress modeling of turbulent open-channel flows". In *Water Resources Research Progress*. Seoul, South Korea.

da Silva Holanda, P., Blanco, C.J.C., Mesquita, A.L.A., Junior, A.C.P.B., de Figueiredo, N.M., Macêdo, E.N. and Secretan, Y., 2017. "Assessment of hydrokinetic energy resources downstream of hydropower plants". *Renewable energy*, Vol. 101, pp. 1203–1214.

de Lima da Silveira e Lorena, M.L.M., 1992. *Meandering Compound Flow*. Ph.D. thesis, University of Glasgow, Glasgow, Scotland.

Farshi, F., Kabiri-Samani, A., Chamani, M. and Atoof, E., 2018. "Evaluation of the secondary current parameter and depth-averaged velocity in curved compound open channels". *Journal of Hydraulic Engineering*, Vol. 144, p. 04018059.

Güney, M. and Kaygusuz, K., 2010. "Hydrokinetic energy conversion systems: A technology status review". *Renewable and Sustainable Energy Reviews*, Vol. 14, pp. 2996–3004.

Guo, Y., Jing, H. and Li, C., 2009. "Numerical simulation of compound meandering open channel flow". In *33rd IAHR Congress*. Aberdeen, Scotland.

Holanda, P.d.S., Blanco, C.J.C., Mesquita, A.L.A., Brasil Junior, A.C.P., de Figueiredo, N.M., Macêdo, E.N. and Secretan, Y., 2017. "Assessment of hydrokinetic energy resources downstream of hydropower plants". *Renewable Energy*, Vol. 101, pp. 1203–1214.

Jing, H., Guo, Y., Li, C. and Zhang, J., 2009. "Three-dimensional numerical simulation of compound meandering open channel flow by the reynolds stress model". *International Journal for Numerical Methods in Fluids*, Vol. 59, No. 8, pp. 927–943.

Jing, H., Li, C., Guo, Y. and Xu, W., 2011. "Numerical simulation of turbulent flows in trapezoidal meandering compound open channels". *International Journal for Numerical Methods in Fluids*, Vol. 65, No. 9, pp. 1071–1083.

Kamel, B., Ilhem, K., Ali, F. and Abdelbaki, D., 2014. "3d simulation of velocity profile of turbulent flow in open channel with complex geometry". In *8th International Conference on Material Sciences, CSM8-ISM5 2012*. Batna, Algeria.

Khan, M., Bhuyan, G., Iqbal, M. and Quaicoe, J., 2009. "Hydrokinetic energy conversion systems and assessment of horizontal and vertical axis turbines for river and tidal applications: A technology status review". *Applied energy*,

Vol. 86, pp. 1823–1835.

Knight, D. and Sellin, R., 2007. "The serc flood channel facility". *Water and Environment Journal*, Vol. 1, pp. 198 – 204.

Knight, D., Wright, N. and Morvan, H., 2005. "Guidelines for applying commercial cfd software to open channel flow". *Report based on research work conducted under EPSRC Grants GR*, Vol. 31, p. 43716.

Laws, N.D. and Epps, B.P., 2016. "Hydrokinetic energy conversion: Technology, research, and outlook". *Renewable and Sustainable Energy Reviews*, Vol. 57, pp. 1245–1259.

Liu, Y. and Packey, D.J., 2014. "Combined-cycle hydropower systems–the potential of applying hydrokinetic turbines in the tailwaters of existing conventional hydropower stations". *Renewable energy*, Vol. 66, pp. 228–231.

Office, W.P.T., 2021. "How hydropower works". Office of Energy Efficiency Renewable Energy, How Hydropower Works, https://www.energy.gov/eere/water/how-hydropower-works. Accessed 28 june 2021.

S.A., P.S., 2015. "Fontes de energia renováveis: Tudo o que você precisa saber (in portuguese)". PORTAL SOLAR S.A., https://www.portalsolar.com.br/fontes-de-energia-renovaveis.html. Accessed 18 june 2021.

Sahoo, A., Samantaray, S. and Bikram Singh, R., 2020. "Analysis of velocity profiles in rectangular straight open channel flow". *Pertanika Journal of Science and Technology*, Vol. 28, pp. 1–18.

Santos, I., Camacho, R.G.R., Tiago Filho, G.L., Botan, A.C.B. and Vinent, B.A., 2019. "Energy potential and economic analysis of hydrokinetic turbines implementation in rivers: An approach using numerical predictions (cfd) and experimental data". *Renewable Energy*, Vol. 143, pp. 648–662.

Tang, L., Sun, H. and Liu, Q., 2015. "Research development of the interaction between turbulence structure and bedforms in open channel". *Advances in Science and Technology of Water Resources*, Vol. 35, pp. 77–84.

Yuce, M.I. and Muratoglu, A., 2015. "Hydrokinetic energy conversion systems: A technology status review". *Renewable and Sustainable Energy Reviews*, Vol. 43, pp. 72–82.

7. RESPONSIBILITY NOTICE

The following text, properly adapted to the number of authors, must be included in the last section of the paper: The author(s) is (are) solely responsible for the printed material included in this paper.